International Journal of Pharmaceutics: X 7 (2024) 100249

Contents lists available at ScienceDirect

International Journal of Pharmaceutics: X

journal homepage: www.sciencedirect.com/journal/international-journal-of-pharmaceutics-x

A drug repurposing approach of Atorvastatin calcium for its antiproliferative activity for effective treatment of breast cancer: *In vitro* and *in vivo* assessment

Dina M. Gaber [a,*], Sherihan S. Ibrahim [b], Ashraf K. Awaad [c], Yasmine M. Shahine [d], Salma Elmallah [e], Hebatallah S. Barakat [f], Noha I. Khamis [g]

[a] *Pharmaceutical Sciences Division (Pharmaceutics), College of Pharmacy, Arab Academy for Science, Technology and Maritime Transport, Abu Kir Campus, Alexandria 1029, Egypt*
[b] *Department of Pharmacology and Therapeutics, Faculty of Pharmacy, Pharos University Alexandria, 21311, Egypt*
[c] *Center of Excellence for Research in Regenerative Medicine and Applications, Faculty of Medicine, Alexandria University, Alexandria 21514, Egypt*
[d] *Department of Microbiology & Immunology, Faculty of Pharmacy, Pharos University, Alexandria 21311, Egypt*
[e] *Pharmaceutical Sciences Division (Pharmaceutical Chemistry), College of Pharmacy, Arab Academy for Science, Technology and Maritime Transport, Abu Kir Campus, Alexandria 1029, Egypt*
[f] *Department of Pharmaceutics, Faculty of Pharmacy, Alexandria University, Alexandria 21525, Egypt*
[g] *Department of Pharmaceutics and Pharmaceutical Technology, Faculty of Pharmacy, Pharos University, Alexandria 21311, Egypt*

ARTICLE INFO

Keywords:
Breast cancer
Drug reprofiling
Active-targeting
Antineoplastic

ABSTRACT

Breast cancer, the most common cancer among women, caused over 500,000 deaths in 2020. Conventional treatments are expensive and have severe side effects. Drug repurposing is a novel approach aiming to reposition clinically approved non-cancer drugs into newer cancer treatments. Atorvastatin calcium (ATR Ca) which is used for the treatment of hypercholesterolemia has potential to modulate cell growth and apoptosis. The study aimed at utilizing gelucire-based solid lipid nanoparticles (SLNs) and lactoferrin (Lf) as targeting ligand to enhance tumor targeting of atorvastatin calcium for effective management of breast cancer. Lf-decorated-ATR Ca-SLNs showed acceptable particle size and PDI values <200 nm and 0.35 respectively, entrapment efficiency >90% and sustained drug release profile with 78.97 ± 12.3% released after 24 h. *In vitro* cytotoxicity study on breast cancer cell lines (MCF-7) showed that Lf-decorated-ATR Ca-SLNs obviously improved anti-tumor activity by 2 to 2.5 folds compared to undecorated ATR Ca-SLNs and free drug. Further, *In vivo* study was also carried out using Ehrlich breast cancer model in mice. Caspase-3 apoptotic marker revealed superior antineoplastic and apoptosis-inducing activity in the groups treated with ATR Ca-SLNs either decorated/ undecorated with Lf in dosage 10 mg/kg/day $p < 0.001$ with superior activity for lactoferrin-decorated formulation.

1. Introduction

Breast cancer is the principal cause of cancer-related fatalities in women worldwide (Misganaw et al., 2023), with an approximated 2.3 million new incidences reported globally in 2020 (Sung et al., 2021). Based on the latest WHO report, it has the second highest incidence of reported cases among all cancer types, accounting for 15% of total deaths among women (Bhagwat et al., 2020). Consequently, breast cancer is currently one of the most focused areas of interest for research (Devi et al., 2020). Despite advances in treatment, metastatic breast

Abbreviations: ATR Ca, Atorvastatin calcium; G 50/13, Gelucire 50/13; Cp, Compritol 888; Lf, Lactoferrin; ATR Ca-SLNs, Atorvastatin calcium loaded solid lipid nanoparticles; Lf-ATR Ca-SLNs, Lactoferrin decorated- Atorvastatin calcium loaded solid lipid nanoparticles; ATR Ca-L-SLNs, Atorvastatin calcium loaded solid lipid nanoparticles at a dose of 5 mg/kg/day; ATR Ca-M-SLNs, Atorvastatin calcium loaded solid lipid nanoparticles at a dose of 10 mg/kg/day; Lf-ATR Ca-L-SLNs, Atorvastatin calcium loaded solid lipid nanoparticles coated with lactoferrin at a dose of 5 mg/kg/day; Lf-ATR Ca-M-SLNs, Atorvastatin calcium loaded solid lipid nanoparticles coated with lactoferrin at a dose of 10 mg/kg/day; Cou 6-SLNs, Coumarin 6-loaded solid lipid nanoparticles; Lf-Cou 6-SLNs, Lactoferrin decorated-coumarin 6-loaded solid lipid nanoparticles; DMEM, Dulbecco's Modified Eagle's Medium.

* Corresponding author at: Division of Pharmaceutical Sciences (Pharmaceutics), College of Pharmacy, Arab Academy for Science, Technology and Maritime Transport, Abu Kir Campus, P.O. Box 1029, Egypt.
E-mail address: dinagaber@aast.edu (D.M. Gaber).

https://doi.org/10.1016/j.ijpx.2024.100249
Received 20 January 2024; Received in revised form 18 April 2024; Accepted 19 April 2024
Available online 20 April 2024

cancer remains incurable and fatal. Subsequently, early detection is crucial for successful treatment, favorable prognosis and high survival rates. Based on the subtype of the tumor and the levels of biological severity of the disease, the main conventional treatment options encompass chemotherapy, radiotherapy, immunotherapy, and surgery (Kafle et al., 2022). Chemotherapy is the gold standard, but the fact that it lacks discriminatory abilities and thus exhibits toxicity in off-target sites poses significant clinical problems and barriers against their effective implication in breast cancer management (Talaat et al., 2022; Was et al., 2022). Besides, drug resistance, fast clearance, and limited bioavailability also pose challenges (Talaat et al., 2022) (Cheng et al., 2021). Further, malignant cells need to lose their chemo protective characteristics and increase their apoptotic rate for significant therapeutic outcomes (Dean et al., 2005). Therefore, there is a need for innovative anticancer treatment strategies, including new synthetic analogues of existing drugs, immunotherapy, repurposed drugs, or using combination drugs.

Drug repurposing, also known as drug repositioning or reprofiling, is a method used to discover new medicinal applications for existing licensed medications, often used to expedite the development process, as the safety and effectiveness of these drugs have been proven (Pushpakom et al., 2019). The market cost of reprofiled pharmaceuticals is around $300 million compared to $2–3 billion required to approve a new drug entity (Nosengo, 2016), offering affordable access to medicines for prevalent disorders like hypertension, diabetes mellitus, and hypercholesterolemia, compared to the estimated cost of a new chemical entity (Malik et al., 2022).

Atorvastatin calcium (ATR Ca) is a synthetic statin that is used mainly for the treatment of hypercholesterolemia. They are Hydroxymethylglutaryl-coenzyme A (HMG-CoA) reductase inhibitors, which block the rate-limiting enzyme in the production of mevalonates, which are precursors to cholesterol biosynthesis. However, statins usually suffer from low systemic bioavailability after oral administration this might be due to pre-systemic elimination by gastrointestinal mucosa and first pass metabolism (Gambhire et al., 2018). On the other hand, Statins have pleiotropic effects, controlling cell proliferation, death, and inflammation, and suppressing cholesterol production, but can also affect disease processes, including cancer, by modulating these pathways (Lochhead and Chan, 2013). Moreover, their anticancer impact on several cell lines, that is related to the inhibition of mevalonate production and its consequences such as cell growth suppression and induction of apoptosis (Mekhail et al., 2012; Osmak, 2012). Atorvastatin have been selected to be used in our study as it is lipophilic in nature, so it possesses a great ability to penetrate the cell membrane as well as high pro-apoptotic activity. Further, atorvastatin as a lipophilic statin has high cytotoxic potential which could be beneficial in cancer treatment (Jiang et al., 2021). Many studies highlighted the effectiveness of atorvastatin in modulating experimentally induced breast cancer in different models as well as in patients (El-Khashab, 2021; Jiang et al., 2021; Liu et al., 2009; Ma et al., 2019). Compared with hydrophilic statins (such as pravastatin and rosuvastatin), lipophilic statins (such as atorvastatin) show a greater ability to penetrate the cell membrane and possess higher pro-apoptotic activity. Furthermore, due to their higher cytotoxic potential, lipophilic statins may be beneficial in cancer treatment (Jiang et al., 2021). In addition, it was reported that ATR Ca could be a promising candidate to be used for efficient suppression of the metastasis of breast cancer (Xu et al., 2014).

Wong and his coworkers (Wong et al., 2007) enhanced oral bioavailability of ATR Ca by its encapsulation into solid lipid nanoparticles (SLNs) as they bypass the liver and is taken up by lymphatic route (Wong et al., 2007). Similarly, Gambhire et al.'s research team (Gambhire et al., 2018) used ATR Ca in nanostructured lipid carriers (NLCs) with a 90% entrapment efficiency. They examined its anti-cancer effects on MCF-7 cell lines for an anticancer investigation. The anticancer activity of atorvastatin-loaded nanostructured lipid carriers (ATR-NLCs) was compared to plain atorvastatin solution and adriamycin, (a widely recognized cytotoxic drug). It was found that, a concentration of 27.4 μg/mL of ATR-NLCs is required for total growth inhibition for MCF-7 cell lines. This concentration is lower than the concentrations of plain atorvastatin (43 μg/mL) and adriamycin (30 μg/mL) necessary for the same effect. These results support the idea that atorvastatin loaded NLCs show promise as an innovative delivery strategy for treating breast cancer (Gambhire et al., 2018).

As a proof of concept, Nanodrug delivery has been proven to improve the therapeutic effectiveness of anticancer medicines by improving drug bioavailability, release pattern, and circulation time (Cheng et al., 2021). Solid lipid nanoparticles (SLNs) are compelling lipid-based colloidal carriers that improve oral drug bioavailability by absorbing through the lymphatic pathway after oral administration (Zhang et al., 2012). SLNs can selectively extravasate into tumor sites due to submicron-sized particulate, enhance permeability and retention, and enable passive tumor targeting (Wong et al., 2007). They are safe, easy-to-manufacture, and effective nanodrug delivery systems made of lipids. They have low drug leakage and good encapsulation effectiveness for hydrophobic medicines related to other nanocarriers such as nanoemulsions and liposomes (da Rocha et al., 2020; Nour et al., 2023). Besides, the slow degradation of solid lipids used in SLN synthesis aids in the extended release of loaded medicines, making SLNs widely used as nanocarriers for cancer treatment (Yaghmur and Mu, 2021). Curcumin inclusion in SLNs, for example, increased its cellular cytotoxicity and absorption against the SKBR3 breast cancer cell line (Wang et al., 2018). In addition, as compared to free Myricetin, SLNs boosted the anti-cancer impact of Myricetin against the A549 lung cancer cell line (Nafee et al., 2020).

Modified therapies can be developed by finding novel ligands targeting malignant cells in combination with anti-cancer drugs to overcome resistance to chemotherapeutic drugs, particularly in breast cancer. Surface modification of nanocarriers with different ligands targeting overexpressed cancer receptors can lead to effective cellular uptake, selectivity, decreased drug clearance to healthy organs, and reduced toxicity of therapeutic actives (Etman et al., 2020). Lactoferrin (Lf), a biodegradable, hydrophilic iron binding glycoprotein, is an extensively used targeting ligand and has been studied for its anticancer properties as an antiproliferative, apoptotic, and antimetastatic agent (Elzoghby et al., 2020; Gibbons et al., 2015). In addition, cancer cells internalize Lf through interactions with low density lipoprotein receptor-related proteins (LRP1 and LRP2) and transferrin binding receptors (TFR1 and TFR2). The cationic nature of Lf enhances cellular uptake by interacting with negatively charged glycosaminoglycans on the cell surface (Elzoghby et al., 2020).

The current study aimed to develop actively targeted solid lipid nanoparticles loaded with atorvastatin calcium and decorated with Lf as a targeting ligand and study its anticancer activity on MCF-7 cell lines and *in vivo* Ehrlich-induced breast cancer model. The anticancer activity of ATR Ca-loaded lipid nanoparticles (decorated/undecorated with Lf) was also compared with plain ATR Ca suspension.

2. Material and methods

2.1. Materials

The sample of atorvastatin calcium, which had a purity of 99.56%, was generously provided by Pharaonia Pharmaceuticals in Alexandria, Egypt. Free samples of lipids, namely Gelucire 50/13 and Compritol 888 ATO, were obtained from Gattefosse in Lyon, France. Lipoid GmbH, located in Ludwigshafen, Germany, provided soybean phosphatidylcholine with a purity level above 96%. Polysciences Europe GmbH, located in Hirschberg, Germany, provided the substance Coumarin-6. The blue-fluorescent stain Hoechst 33342, which is used specifically to stain DNA (*i.e.*, the nuclei of eukaryotic cells), was obtained from Thermo Fisher Scientific in the United States. The lactoferrin sample was generously provided by Sigma Aldrich, in Schnelldorf, Germany. O-

Table 1
Composition of Lf-decorated/ undecorated blank, drug loaded and fluorescently labelled SLNs.

Concentration / SLNs dispersion (% *w/v*)						
Formula code	Drug	Fluorescent dye	Lipids		Phospholipid	Targeting ligand
	ATR Ca	Cou 6	G 50/ 13	Cp 888	Lipoid s 100	(Lf)
Blank SLNs	__	__	2.0	0.5	2.0	__
Lf- Blank-SLNs	__	__	2.0	0.5	2.0	1.0
ATR Ca-SLNs	0.2	__	2.0	0.5	2.0	__
Lf-ATR Ca-SLNs	0.2	__	2.0	0.5	2.0	1.0
Cou 6-SLNs	__	0.001	2.0	0.5	2.0	__
Lf-Cou 6-SLNs	__	0.001	2.0	0.5	2.0	1.0

phosphoric acid and acetonitrile (HPLC grade) were obtained from Merk in Massachusetts, USA. The potassium dihydrogen phosphate was supplied by El-Nasr Pharmaceutical Co. in Cairo, Egypt. The MCF-7 breast cancer cell line was acquired from the Centre of Excellence for Regenerative Medicine and Its Applications, Faculty of Medicine, Alexandria University, Egypt. The Dulbecco's modified eagle medium (DMEM) was acquired from Sigma-Aldrich Corporation, located in St. Louis, Missouri, USA. The fetal bovine serum (FBS) was received from Biowest, which is located in Nuaillé, France. The procurement of Penicillin/Streptomycin was done from Life Technologies, located in Carlsbad, *CA*. The immunohistochemistry analysis utilized kits and antibodies, including Hydrogen Peroxide Block, Biotinylated Goat Anti-Polyvalent, and Streptavidin Peroxidase, which were procured from Thermofisher Biochemicals, USA. The sodium citrate was acquired from Elgomhoria chemicals, located in Egypt. The Rabbit Polyclonal Antibody Caspase 3 (CPP32) Ab-4 (5 μg/mL) was obtained from Neo Markers-Lab Vision Corporation, USA. Skytek Laboratories provided DAB Plus Chromogen and DAB Plus substrate.

2.2. Formulations of delivery systems

2.2.1. Preparations of blank nanoparticles with/ without lactoferrin

Solid lipid nanoparticles (SLNs) were prepared using hot high sheer homogenization technique as previously reported by Nafee et al. (Nafee et al., 2020) with slight modifications. Briefly, solid lipids Gelucire 50/ 13, Comperitol, Lipoid S100 in concentrations 2.0, 0.5 and 2% *w/v*, respectively were melted in water bath at 80 °C. Then Milli-Q water that has been previously heated was added slowly under magnetic stirring at 300 rpm. Furthermore, the nanodispersion underwent high-shear homogenization at 10,000 rpm for 10 min in a water bath at 80 °C, followed by probe sonication for 3 min at 50% amplitude at similar temperature. Lastly, the SLNs were congealed by cooling with stirring at 300 rpm. Lactoferrin decorated particles were prepared by adding Lf (1% *w/v*) in a dropwise manner to 10 mL of the SLNs dispersion under continued stirring at 300 rpm for 45 min. Different formulations are shown in Table 1.

2.2.2. Preparation of ATR Ca-SLNs with/ without Lf

The SLNs loaded Atorvastatin calcium (ATR Ca) either decorated or undecorated with Lf as a target ligand were prepared. All lipids were thawed in water bath at temperature 80 °C, later ATR Ca was dissolved in the melted lipids followed by addition of Milli Q water at the same temperature and the rest of preparation procedure proceed as described in the previous section. The composition of all formulations is illustrated in Table 1. In addition, for *in vitro* cellular uptake, to allow visualization of SLNs by confocal laser scanning microscope, Lf decorated/ undecorated fluorescently labelled SLNs were prepared as described above with substituting ATR Ca with coumarin 6 (λ_{ex} 450 nm, λ_{em} 505 nm) in concentration 0.001%w/v.

2.3. HPLC analysis of ATR Ca

2.3.1. Calibration curve

Standard stock solution of ATR Ca in acetonitrile was prepared at a concentration equivalent to 1 mg/mL w/v. Consecutively, working solutions with concentrations ranging from of 0.125–2.0 mg% w/v were prepared for the construction of the calibration curve *via* diluting of the stock solution. The ATR Ca serial dilutions were prepared by taking different quantities from stock solution, diluting with mobile phase (Acetonitrile: 1.36 g/L potassium dihydrogen phosphate and adjusting the pH at 3.2 using O-Phosphoric acid) (60:40 *v*/v).

2.3.2. Chromatographic conditions and construction of calibration curve

A system with a reverse phase Kromasil-C18 column was used to perform the HPLC analysis of ATR Ca-SLN formulations. A sequence of Acetonitrile: 1.36 g/L potassium dihydrogen phosphate adjusted to pH 3.02 using O-Phosphoric acid (60:40 v/v) was used as the isocratic mobile phase and eluted at a flow rate 2 mL/min. Twenty microliters were used as the injection volume. The elution from 190 to 400 nm was monitored using the diode array detector and the chromatograms were withdrawn at 235 nm. The temperature was set at 26 °C while recording all measurements. Triplicate injections were conducted and chromatographed for each concentration using the aforementioned conditions.

2.4. Characterization of delivery systems

2.4.1. Colloidal properties and Morphology

The Nano-Zetasizer, manufactured by Malvern Instruments UK, was utilized to evaluate the particle size distribution and surface charge of NPs that have been diluted with Milli Q, as previously documented by Gaber et al. (Gaber et al., 2017). The average and standard deviation of three measurements is used to calculate the findings. Further, the morphology of blank and drug-loaded solid lipid nanoparticles (SLNs), with or without lactoferrin (Lf) decoration, was observed using transmission electron microscopy (TEM, model JEM-100CX, JEOL, Japan) following negative staining with uranyl acetate.

2.4.2. Entrapment of ATR Ca and invitro drug release

2.4.2.1. Entrapment efficiency. ATR Ca-loaded SLNs with/ Without LF were abstracted from unencapsulated ATR Ca by centrifugal ultrafiltration using Centrisart-I®, MWCO 20 kDa. One mL of SLN dispersion was added in Centrisart-I® and centrifuged using centrifuge at speed 4000 rpm for 10 min. Methanol was used as solvent to extract the encapsulated ATR Ca from purified loaded SLNs which was then quantified by HPLC method as previously described in section 2.3.2. Each sample was carried out in triplicates.

2.4.2.2. In vitro drug release study. The *in vitro* release of both ATR Ca-SLNs and Lf-ATR Ca-SLNs was examined compared to free drug suspension in water. In brief, 2 mL of freshly made SLNs suspension (equivalent to 4 mg ATR Ca) was introduced into a dialysis bag (molecular weight cutoff 12,000). The bag was then placed in a flask containing 100 ml phosphate buffer (pH 7.4): ethanol (60:40). The flask was maintained at a temperature of 37 ± 0.5 °C in a water bath that was set to shake at a speed of 100 rpm. One mL of dispersion was removed and substituted with equal volume of fresh medium to preserve sink condition. The samples are diluted (1:1) with mobile phase and assayed by previously mentioned HPLC method in section 2.3.2. Each release study

was conducted three times.

2.5. In vitro assessment on cell culture model

The MCF7 cell lines obtained were certified to be Mycoplasma-free and the experiment was done in strictly sterile conditions. MCF-7 cells were cultured in Dulbecco's modified Eagle medium, supplemented with 10% heat-inactivated fetal bovine serum and 1% *v*/v Penicillin/ Streptomycin. The cells were incubated in a CO2 incubator at 37 °C with a humidified atmosphere containing 5% CO2. The cells were placed in a 96-well plate with a density of 5×10^3 cells per well. Each well contained 100 μL of DMEM. The cells were left to attach to the plate overnight.

2.5.1. In vitro Cell Viability Assay

As a proof of concept to verify the function of ATR Ca for its antitumor activity, and the role of Lf in enhancing antitumor activity of ATR Ca SLNs, MTT viability assay was conducted on MCF-7 cells.

2.5.2. Samples and control

The samples to be assessed included ATR Ca-SLNs and Lf-ATR Ca-SLNs in increasing ATR Ca concentrations (0.6, 3, 6, 12, 30, 45, and 60 μg/mL). In parallel, the equivalent blank particles and free ATR Ca solution were tested. Positive and negative controls comprised of untreated cells and cells treated with Triton X (1% *w/v*) ($n = 6$), respectively. Vehicle control (DMEM), substance control (SLNs + assay reagents) and DMSO (0.5% *v*/v) served as further controls.

2.5.3. MTT Viability Assay Protocol

Samples were first diluted in DMEM, thenceforth samples were added in triplicate to MCF-7 cells and incubated for 24 h. Thenceforward samples were discarded, and cells were washed twice with PBS following the incubation period. MTT reagent (5 mg/mL PBS) was added for 4 h to assess the cells viability. Later, 100 μL dimethyl sulfoxide (DMSO) were used to solubilize the formazan crystals which were later quantified spectrophotometrically at 570 nm using microplate reader (SunRise, TECAN Inc., USA). The following equation was used to determine the percentage of cell viability compared to control cells incubated with culture medium only:

$$\%\text{Cell viability} = \left[\frac{\text{A (Test)} - \text{A (Negative control)}}{\text{A (Positive control)} - \text{A (Negative control)}} \right] * 100 \quad (1)$$

Table 2
The treatment regimen protocol for different mice groups.

Group #	Group name	Description
Group 1	Negative Control	Healthy mice.
Group 2	Positive Control	untreated Ehrlich-induced solid breast cancer mice injected IP with Saline.
Group 3	SLNs	Mice injected IP with blank solid lipid nanoparticles.
Group 4	Lf-SLNs	Mice injected IP with blank solid lipid nanoparticles decorated with lactoferrin.
Group 5	ATR Ca-L	Mice injected IP atorvastatin-calcium free drug at a dose of 5 mg/kg/day.
Group 6	ATR Ca-M	Mice injected IP atorvastatin-calcium free drug at a dose of 10 mg/kg/day.
Group 7	ATR Ca-L-SLNs	Mice injected IP with atorvastatin-calcium solid lipid nanoparticles at a dose of 5 mg/kg/day.
Group 8	ATR Ca-M-SLNs	Mice injected IP with atorvastatin-calcium solid lipid nanoparticles at a dose of 10 mg/kg/day.
Group 9	Lf-ATR Ca-L-SLNs	Mice injected IP with atorvastatin-calcium solid lipid nanoparticles decorated with lactoferrin at a dose of 5 mg/kg/day.
Group 10	Lf-ATR Ca-M-SLNs	Mice injected IP with atorvastatin-calcium solid lipid nanoparticles decorated with lactoferrin at a dose of 10 mg/kg/day.

The IC_{50}, which represents the concentration needed to cause 50% cell death, was obtained by analyzing the dose response curve for each concentration using Graphpad Prism 8.1 software (San Diego, CA, USA). The absorbance obtained from the test sample is denoted as A (Test), whereas the absorbance obtained from the 100% death control wells is denoted as A (Negative control). A (Positive control) represents the absorbance obtained from untreated cells that were incubated with medium alone. The latter interpretation was presumed to align with 100% cellular viability. The MTT test was conducted in triplicate for each concentration.

2.6. Localization and Cellular uptake in MCF-7 cells

2.6.1. Confocal Microscopy Study

The cellular uptake tests involved the use of coumarin 6-labelled solid lipid nanoparticles that were either decorated or undecorated with Lf, specifically referred to as Lf-Cou 6-SLNs and Cou 6-SLNs, respectively. These SLNs were compared to a control solution of coumarin-6 in dimethyl sulfoxide (DMSO) at a concentration of 10 μg/mL. Fluorescently labelled SLNs were synthesized using the same method as ATR Ca-SLNs, but with the substitution of ATR Ca with coumarin-6 at a concentration of 10 μg/mL in the SLNs dispersion. The MCF-7 cells, at a density of 0.5×10^5 cells per well, were placed on a 6-well plate that had been sterilized with UV light. The plate was covered with glass and left to incubate overnight. Samples (equivalent to coumarin concentration of 6 ng) were then incubated with the cells for a duration of 24 h. After undergoing multiple washing steps, cells were treated with 4% paraformaldehyde as a fixative, permeabilized with 0.1% Triton X-100 and hence, nuclei were stained in blue with Höchst 33,342. Finally, the cells were examined using confocal laser scanning microscopy (CLSM; Leica TSC SPE II/ DMi 8, Wetzlar, Germany). The fluorescence intensity of the confocal images was determined by processing them using Leica Las-X software (Leica, Wetzlar, Germany). Particle internalization was verified as a proof of concept through the use of 3D-time lapse imaging of *Z*-stacks (14 μm). The Leica Las-X software was utilized for data assessment and 3D reconstruction.

2.6.2. Flow cytometry Study

Cellular uptake was further quantitatively investigated by flow cytometry (BD FACSCalibur, BD Biosciences, USA). Briefly, MCF-7 cells were seeded in a 12-well plate at a seeding density of 5×10^5 cells/ well containing the desired concentration of coumarin-labelled SLNs both decorated/ undecorated with Lf (Lf-Cou 6-SLNs, Cou 6-SLNs) in addition to coumarin-6 solution (10 μg/mL), the desired concentration of coumarin is 6 ng. After 24 h incubation, MCF-7 cells were collected by initially discarding the growth medium, rinsing three times with 1 × PBS, and subsequently exposing them to trypsin solution at a temperature of 37 °C for a duration of 5 min. Consequently, trypsin was inactivated by adding a double volume of cell culture medium containing fetal bovine serum albumin. The entire volume, consisting of trypsin and medium, was placed into a 5 mL flow tube and subjected to centrifugation at 1800 rpm in order to collect the cells in a pellet form. After that, the cell pellet was resuspended in 400 μL of 1 × PBS with light vortexing. All samples were kept on ice while waiting for analysis. Flow cytometry was performed using a BD FACSCalibur (BD Biosciences, USA). The instrument was setup to collect 5000 events per sample. Data for intracellular uptake efficiency, mean fluorescence intensity and cell counts were collected and analyzed from the flow cytometer and plotted in a graph using BD CellQuest Pro software (BD Biosciences, USA).

2.7. In vivo assessment of the formulations' efficacy

2.7.1. Animals

Female Swiss albino mice weighing 20–25 g and 6–7 weeks old were obtained from Pharos University in Alexandria. The mice were then housed with unrestricted access to food and water for a week prior to the

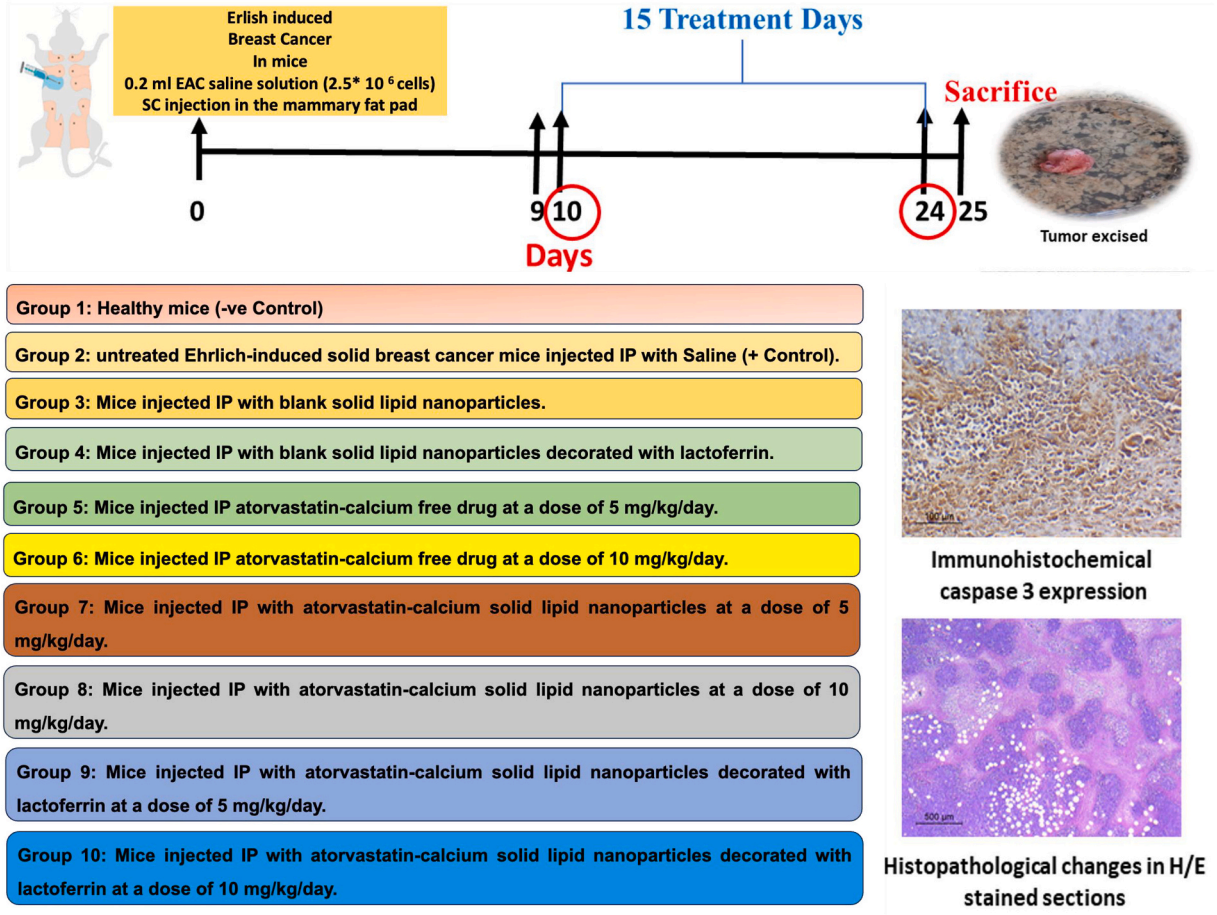

Fig. 1. Timeline of *In vivo* experimental design.

initiation of the *in-vivo* experimental model. The ethics committee at Pharos University in Alexandria (PUA) authorized all experimental procedures *(PUA-01202311263150)*, which were carried out strictly in compliance with the standards for the Care and Use of Laboratory Animals (NIH) and Animal Research: Reporting of *In Vivo* Experiments (ARRIVE).

2.7.2. Ehrlich-induced breast solid tumor

From the Egyptian National Cancer Institute (NCI; Cairo University, Egypt), a mouse with Ehrlich ascites carcinoma (EAC) was obtained. After the ascites solution had been extracted from the mice's peritoneum, tumor cells quantification in the ascites fluid was counted using a Neubauer hemocytometer. After that, the tumor cells' viability was assessed *via* trypan blue assay. The Ehrlich ascites carcinoma cells (EAC) were subsequently reconstituted in phosphate buffer saline (PBS). On day zero, 0.2 mL of EAC saline solution (2.5×10^6 cells) was subcutaneously injected into the mammary fat pad of every animal in the experimental groups. For nine days, mice with unrestricted access to food and water, developed solid breast cancer (Ibrahim et al., 2022).

2.7.3. Experimental animal groups

Every 8 mice were allocated into a group forming 10 different groups according to the following scheme as depicted in Table 2 with drug administration performed intraperitoneally. The doses used in this study were selected based on the results obtained from our pilot experiment that have been done and based on literature (Beckwitt et al., 2018; Liu et al., 2009). Tested drugs were administered daily for 15 days commencing on the 10th day and continuing until the end of the study (Fig. 1).

2.7.4. Assessment of Ehrlich induced solid tumor volume

The tumor volume (V) was assessed using a vernier calliper every other day until the final measurement on day 25. The calculation of the tumor volume was performed by using the following equation (Ibrahim et al., 2022):

$$V = (\text{length} + [\text{width}]2/2 \quad (2)$$

2.7.5. Tumor tissue samples collection

Mice were anesthetized with ketamine and xylazine on the 25th day. Following cervical dislocation, the tumor was excised from each mouse and immediately rinsed with ice-cold saline solution. Subsequently, the tumor was dried by blotting it on filter paper. Finally, the tumor samples were fixed in a 10% formaldehyde solution overnight before being processed to create paraffin-embedded blocks for histopathological and immunohistochemical evaluations (Ibrahim et al., 2022).

2.7.6. Histopathological investigations

Fixed samples underwent dehydration through ascending grades of alcohol, cleared in xylene, and subsequently embedded in paraffin wax. Tissue blocks were then cut into 4–5 μm thick sections that were then deparaffinized. The slides were rehydrated in descending grades of alcohol, and then immersed in tape water. Sections on glass slide were stained with Mayer's Hematoxylin for 7 min, washed, and then counterstained with Eosin for 3 min and processed to be mounted with Canada balsam. The tumor's necrosis was evaluated. Multiple photographs were obtained for at least 5 consecutive fields using the microscope's camera (Leica DMC2900). The photographs were then analyzed using Image J software to determine the proportion of necrotic regions among the whole investigated surface. Structureless deep eosinophilic granular

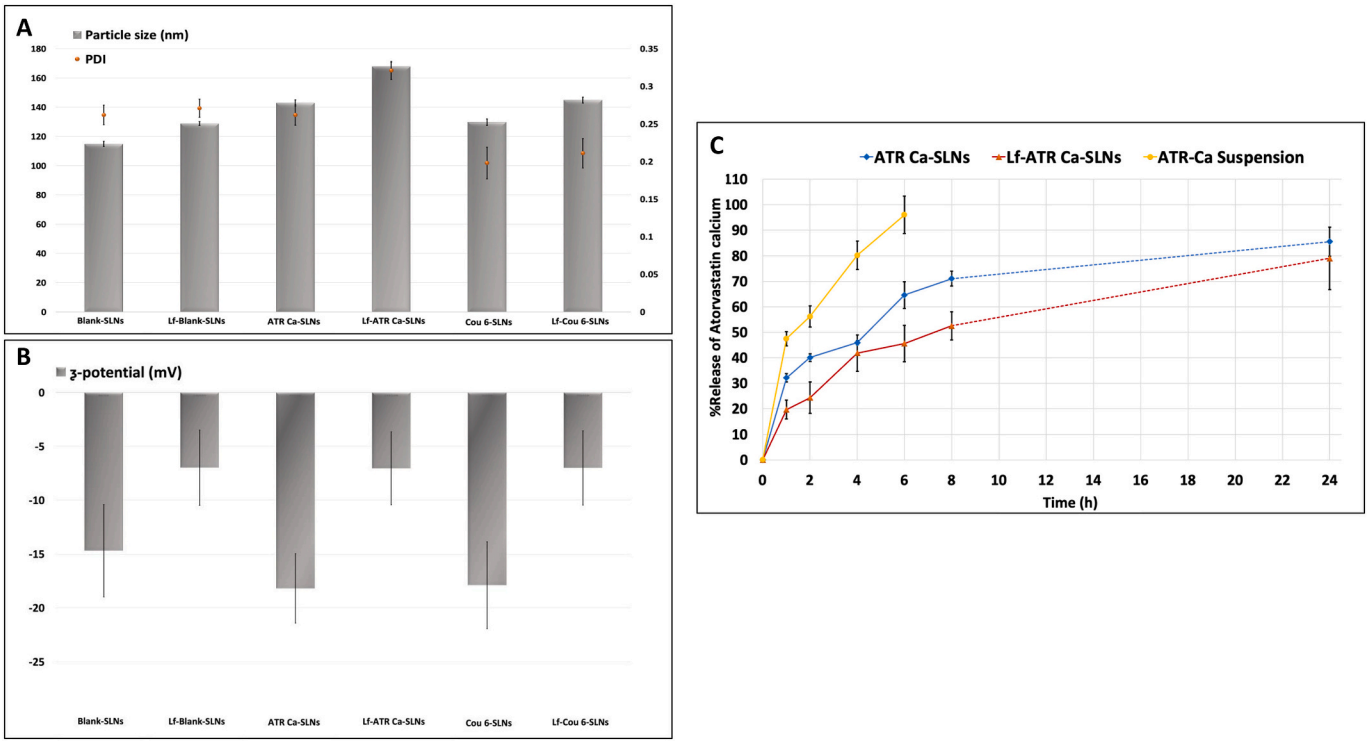

Fig. 2. A. Particle size (nm) and polydispersity index of SLNs formulations. The data shown are the mean values ($n = 3$) ± SD.
B. Zeta potential (mV) of SLNs Formulations. The data shown are the mean values (n = 3) ± SD.
C. *In vitro* release of ATR Ca from: ATR Ca-SLNs, and Lf-ATR Ca-SLNs in (Acetonitrile: 1.36 g/l potassium dihydrogen phosphate and adjusted to pH 3.2 with O-Phosphoric acid (60:40). Each point represents the mean (n = 3) ± SD.

regions with cellular and nuclear debris were seen in necrotic areas (Naik et al., 2020).

2.7.6.1. Immunohistochemical detection of caspase 3 level:. The identification of Caspase-3 was accomplished by a semi-quantitative method utilizing a rabbit polyclonal IgG LabVision (Caspase 3 (CPP32) Ab-4) and a labelled streptavidin-biotin immunoenzymatic antigen detection system (Ultra Vision Detection System, Anti-Polyvalent, HRP/DAB), following the instructions provided by the manufacturer.

Tissue sections were deparaffinized and rehydrated, and then Slides were then incubated in 3% hydrogen peroxide block for 10–15 min. Sections were then immersed in retrieval sodium citrate buffer 0.01 M, pH: 6.0 then heated at 100 °C, slides were then cooled at room temperature and washed with PBS. Normal goat serum diluted 1: 5 in PBS was then added to the tissue sections and incubated for 30 min. The sections were covered with diluted Rabbit Polyclonal Antibody Caspase 3 (CPP32) Ab-4 (5 µg/mL) and incubated overnight at temperature 4 °C in a humid chamber. Biotinylated Goat Anti-Polyvalent was applied and the slides were incubated for 10 min at room temperature. Slides were then washed 4 times in buffer followed by the addition of Streptavidin Peroxidase incubation for 10 min at room temperature. 40 µL of DAB Plus Chromogen was added to 2 mL of DAB Plus substrate and then applied to the tissue. The slides were finally counterstained in Mayer's hematoxylin and coverslip using a permanent mounting media (Abou Shousha et al., 2023). The DAB chromogen produces a brown color reaction end product at the site of target antigen, and the immunostaining was evaluated using a semi-quantitative scale. The tumor samples were graded as negative when there was complete absence of nuclear or cytoplasmic staining (0). The positive tumor samples were graded as weak (1), moderate (2), and strong (3) based on the intensity of nuclear staining and/or cytoplasmic (Knoblaugh and Himmel, 2019).

2.8. Statistical analysis

The data were subjected to statistical analysis using the GraphPad Prism 0.8 (GraphPad Software Inc., USA). Correlations were used to analyze different parameters. Descriptive analysis was used in the terms of mean ± standard deviation, ($n = 8$ mice/group). Results considered to be significant at P value <0.05. Two-way ANOVA test was used as test of significance followed by Bonferroni as a post hock test for illustrating significance between tumor size of various experimental groups on day 25. The immunohistochemical scores were analyzed using Kruskal-Wallis test followed by Dunn's post-test.

3. Results and discussion

3.1. HPLC analysis of ATR Ca

The ATR Ca concentration was determined using a High-Performance Liquid Chromatography (HPLC) technique. The chromatogram in Fig. S1(Supplementary data) displayed a concentration of 0.5 mg% *w/v* of ATR Ca solution, which was diluted with a mobile phase. Furthermore, it exhibits a symmetrical and distinct peak with a retention duration of 4.09 min. A graph displaying the relationship between the peak area at 235 nm and the corresponding drug concentration, known as a calibration curve. The calibration curve exhibited a strong linear correlation (R2 = 0.9994) across a range of ATR Ca concentrations, namely from 0.125 to 2 mg% w/v, as shown in Fig. S2 (Supplementary data).

3.2. Colloidal properties and surface morphology

Fig. 2A and B depicts the impact of payload (ATR Ca/ Coumarin 6) and surface decoration with Lf on the colloidal properties of SLNs formulations. Surfactant free gelucire-based SLNs were around 114.9 ±

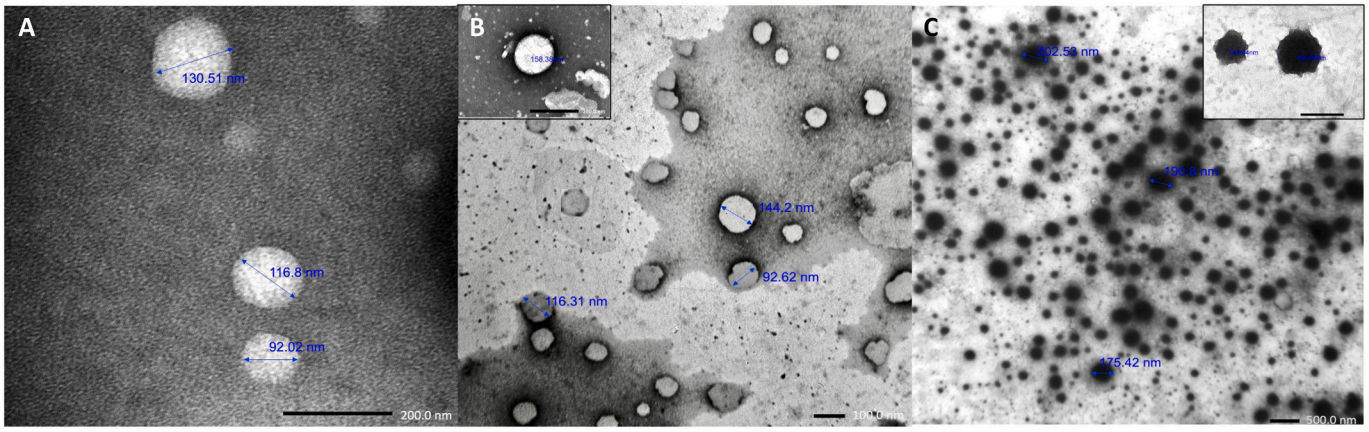

Fig. 3. TEM Photo microphotograph of: (A) Plain SLNs, (B) ATR Ca-SLNs and (C) Lf-ATR Ca-SLNs.

1.25 nm in diameter with negative surface potential (−14.7 ± 4.29 mV). Loading SLNs with either ATR Ca (ATR Ca-SLNs) or coumarin-6 (Cou 6-SLNs) slightly enlarged the particle size with slight corresponding reduction in ʒ-potential up to −18.2 ± 3.22 and − 17.9 ± 4.04 mV, respectively. Surface decoration of nanoparticles with Lf (Lf-ATR Ca-SLNs) changed the ʒ-potential to −7.05 ± 3.39 mV with slight impact on size with an average size of 167.8 ± 0.993 nm.

Further, TEM images showed that SLNs appear spherical with smooth surface and average particle size distribution analogous to size measurements by dynamic light scattering, with no signs of particle aggregation (Fig. 3A). Atr Ca-SLNs did not display any crystals denoting drug encapsulation in the molecular state (Fig. 3B). It is believed that the organization of the lipid matrix, the stabilizing agents and the active ingredient in SLNs together with their relation to one another dictates their behavior as drug carriers (Nafee et al., 2020). Further, coating SLNs with Lf were darker (Fig. 3C) in accordance with photomicrographs were obtained by Shilpi et al. (Shilpi et al., 2015).

3.3. Entrapment efficiency

The drug entrapment efficiency for ATR Ca-SLNs and Lf-ATR Ca-SLNs were 95.6 ± 1.16% and 94.4 ± 1.31%, respectively. This might be due to the use of high-melting solid lipids like G 55/13 and Cp tend to create rigid solid particles with a larger total lipid content, leading to improved drug incorporation (Nafee et al., 2020). This reflects the suitability of the formulation technique, choice of lipid/emulsifier combination and ratio that offer promising incorporation of the payload.

3.4. In vitro drug release

Release profiles of different ATR Ca-SLNs formulations namely ATR Ca-SLNs and Lf-ATR Ca-SLNs were determined in comparison to free drug suspension in water to investigate the impact of formulation on drug release. Drug release was studied in 40% ethanol in phosphate buffer solution, pH 7.4 at 37 °C under sink conditions. The amounts of drug released from the selected formulations in comparison with drug dispersion were plotted as a function of time. Compared to free drug suspension, all ATR Ca-SLNs formulations showed biphasic release patterns with an initial burst release during the first 5 h followed by a more sustained release pattern up to 24 h. On the other hand, owing to its poor aqueous solubility, drug suspension showed somehow sustained drug release with 80.18 ± 5.6% released after 4 h. (Fig. 2C). However, it was evident that inclusion of the drug ATR Ca in SLNs obviously reduced its extent of release where 85.57 ± 5.71% and 78.97 ± 12.3% of drug was released from ATR Ca-SLNs and Lf-ATR Ca-SLNs after 24 h. The reason behind the lower amount of ATR Ca released form Lf-coupled SLNs compared to uncoupled SLNs is Lf might offer substantial

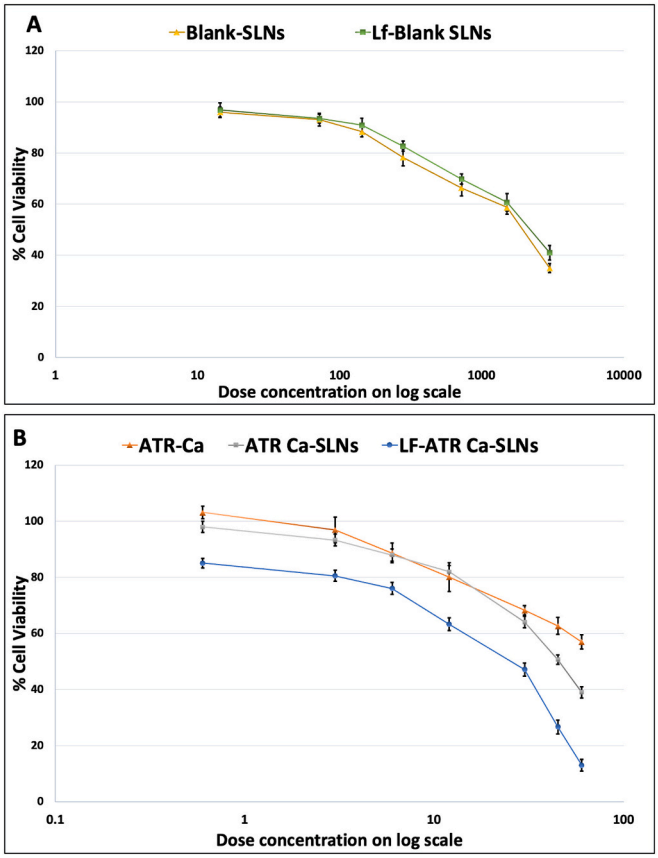

Fig. 4. The vitality percentage of MCF-7 cells was determined using the MTT viability test after being exposed for 24 h to different doses of: (A) Blank SLNs, Lf-Blank SLNs, (B) ATR—Ca, ATR-Ca-SLNs and Lf-ATR-Ca-SLNs at 37 ± 0.5 °C, mean ± SD., (n = 3).

shielding on the surface of SLNs. Some Studies have shown similar release patterns for rifampicin and paclitaxel from uncoupled and Lf-coupled SLNs (Pandey et al., 2015; Shilpi et al., 2015), as well as for methotrexate from lactoferrin–dendrimer conjugates (Lf-PPI) and plain dendrimer (PPI) (Kurmi et al., 2011).

3.5. In vitro cytotoxicity study

The *in vitro* cytotoxicity study for both Lf decorated and undecorated ATR Ca-SLNs was carried out on MCF-7 cells (Abolghasemi et al., 2022;

Table 3
IC_{50} values of SLNs formulations compared to the free drug.

Formula name	IC_{50} (μg /mL)
Blank SLNs	193.4825 ± 2.64
Lf- Blank-SLNs	176.813 ± 3.41
Atorvastatin calcium trihydrate	51.784 ± 3.02
ATR Ca-SLNs	45.718 ± 2.93
Lf-ATR Ca-SLNs	21.8 ± 2.56

Gambhire et al., 2018) for 24 h to study the antitumor effect of ATR Ca as well as the potential of Lf as a targeting ligand on cell viability. Despite the well-established understanding that statins exhibit their anticancer effects in laboratory settings along the epithelial-mesenchymal axis, where mesenchymal cells have greater sensitivity to statins compared to epithelial or hybrid epithelial-mesenchymal tumor cells, (van Leeuwen et al., 2022; Warita et al., 2014). The selection for the MCF7 cell line was based on their classification as a luminal A breast cancer cell line (Moon et al., 2020) which is considered the most common breast cancer molecular subtype in Egypt accounting for >42% of total breast cancer cases (El-Hawary et al., 2012). Added to that, there have been previous studies in the literature that have demonstrated the antitumor effect of ATR against breast cancer using MCF7 cell lines (Abolghasemi et al., 2022; Gambhire et al., 2018).

The results indicated that both blank SLNs formulations, whether decorated with Lf or not, had minimal cytotoxic action. After 24 h of incubation, the percentage of cell viability remained over 70%, (Fig. 4A/ Table 3; IC_{50} values of 193.4825 ± 2.64 μg/mL and 176.813 ± 3.41 μg/mL), for both Blank SLNs and Lf-Blank SLNs, respectively. This validates the cytocompatibility of blank SLNs as a carrier for delivering ATR *Ca.* The IC_{50} of ATR Ca SLNs is less than free ATR Ca as shown in Table 3, which indicates that the concentration of drug required for 50% growth inhibition is less in the case of ATR Ca-SLNs when compared to free drug. The overall results confirm that the cytotoxicity of the drug is increased when formulated in lipid-based formulations. Further, Lf decorated ATR Ca-SLNs were found to exhibit obvious growth inhibition on MCF-7 cells in comparison to undecorated SLNs and free drug (Fig. 4B). Where indeed, 2–2.5 folds lower IC_{50} value was recorded for Lf-ATR Ca-SLNs (21.8 ± 2.56 μg/mL) compared to 51.784 ± 3.02 μg/mL and 45.718 ± 2.93 μg/mL for ATR Ca-SLNs and free ATR Ca, respectively. The improvement in toxicity related to active targeted SLNs can be due to the increased internalization into cells through ligand-receptor interaction.

3.6. *In vitro cellular uptake and colocalization studies in MCF-7 cells*

CLSM examined the cellular uptake of Cou 6-SLNs and Lf-Cou 6-SLNs, in addition to Cou 6 solution in DMSO, on MCF-7 cells over 24 h. CLSM pictures show greater fluorescent signals in cells treated with Cou 6-SLNs, indicating higher absorption levels compared to free dye (Fig. 5A). Furthermore, cells treated with Lf-Cou6-SLNs produced brighter fluorescence signals than cells treated with Cou 6-SLNs and free dye solution, indicating a higher level of internalization and demonstrating the direct influence of ligand targeting on cellular uptake (Fig. 5A). In order to distinguish between the surface binding of SLNs and their internalization inside cells, we employed 3D time lapse imaging. This technique enabled us to capture images of 40 consecutive stacks within cells along the z-direction, spanning a distance of 14 μm (Fig. 5B). The *Z*-stacks confirm particle localization within the cells, particularly in the cytoplasm and seldom in the nucleus. This phenomenon may be attributed to the internalization of nanoparticles by endocytosis, facilitated by their small size at the nanoscale. Specifically, in the case of solid lipid nanoparticles (SLNs), the fusing of these lipid-based particles with the cell membrane enhances the transfer of drugs

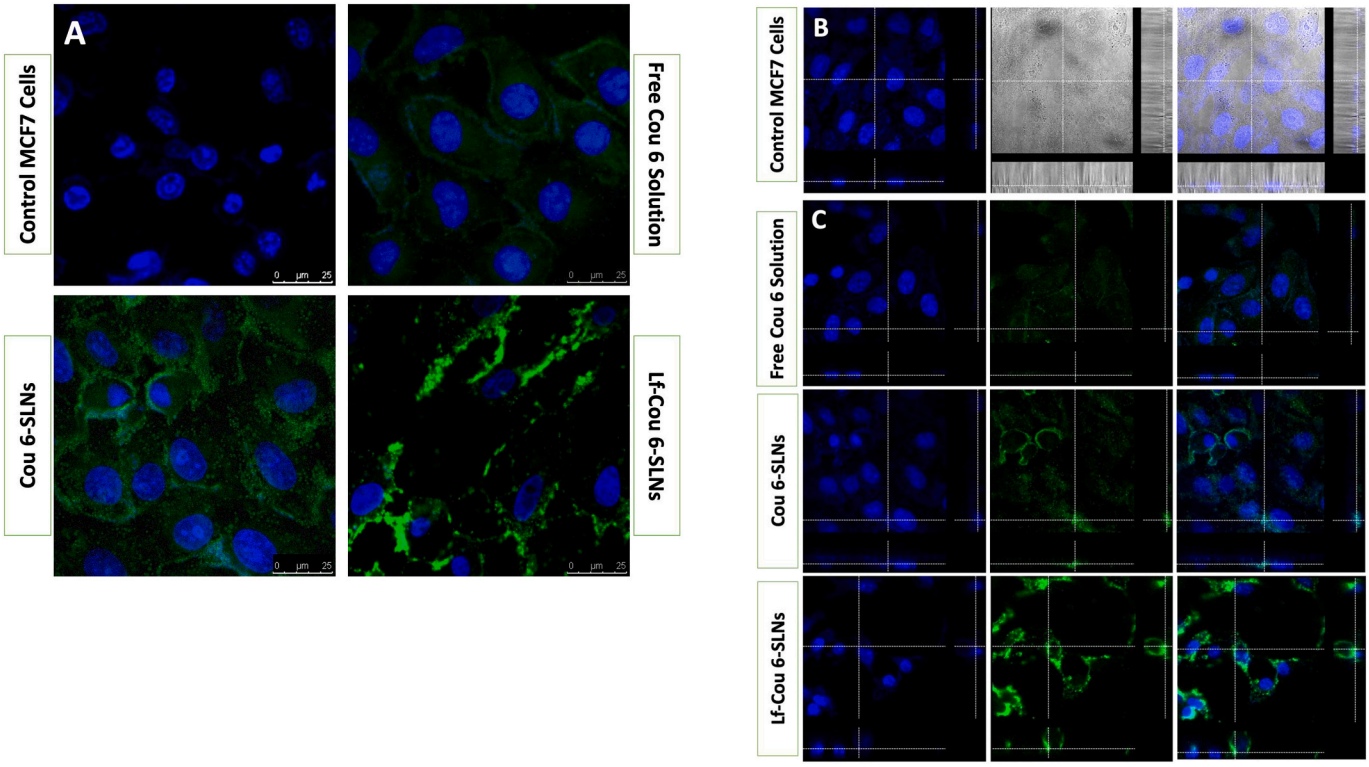

Fig. 5. A. Confocal laser microscopy images of MCF-7 cells incubated with free Cou 6 solution, Cou 6-SLNs and Lf-Cou 6-SLNs (magnification 63×). After 24 h incubation with a suspension of Cou 6 (Green)-containing SLNs (50 and 60 mg/mL) for Cou 6-SLNs and Lf-Cou 6-SLNs, respectively at 37 °C. Scale bar, 25 μm. (For interpretation of the references to color in this figure legend, the reader is referred to the web version of this article.)
B. CLSM *Z*-stack of MCF-7 breast cancer cells.
C. CLSM Z-stacks illustrating the uptake of Cou 6-labelled SLNs *vs.* free dye after 24 h.

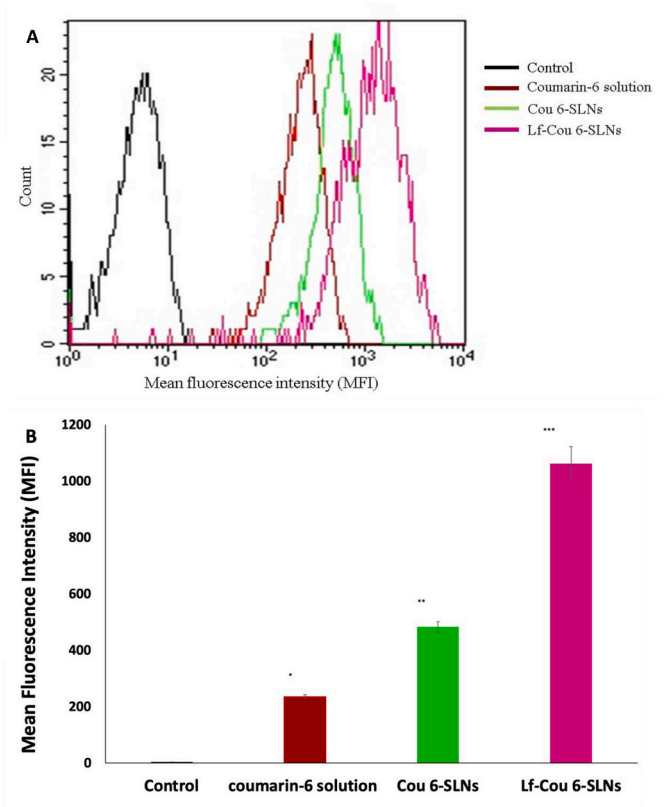

Fig. 6. Assessments of cell uptake efficiency of coumarin 6-labelled SLNs (decorated with and without Lf) into MCF-7 breast cancer cell line by flow cytometry analysis.
A. Representative histograms of MCF-7 cells treated, for 24 h, with Cou 6-SLNs (decorated with and without LF) and Cou-6 solution compared to the untreated control cells.
B. Corresponding quantification of cellular level of MFI in MCF-7 cells. Values are represented by the mean ± standard deviation. The data was analyzed by one-way ANOVA followed by Tukey's post-hoc test. $p < 0.05$ (n = 3).
**Significance between treated groups in comparison to control untreated group.*

from the extracellular to the intracellular regions. (Kulkarni and Feng, 2013; Rivolta et al., 2011). Furthermore, Lf-Cou 6-SLNs were clearly observed with intense green fluorescence and sharper patches inside the cell proximity, suggesting their probable entrapment within intracellular vesicles. This highlights the significance of actively targeting the tumors by using the binding between ligands and receptors in cancer nanotherapeutics.

Flow cytometry analysis was performed for quantitative evaluation of the cellular uptake of coumarin- labelled SLNs both decorated and undecorated with Lf (Lf-Cou 6-SLNs, Cou 6-SLNs) and coumarin-6 solution in comparison to control cells incubated with culture medium only into MCF-7 breast cancer cells (Fig. 6). The cellular uptake efficiency was evaluated as a function of mean fluorescence intensity (MFI) obtained from the flow cytometry data (Fig. 6B). The MFI of SLNs undecorated with Lf (Cou6-SLNs) was a little stronger than that of coumarin-6 solution compared to Control cells. However, in SLNs decorated with Lf (Lf-Cou 6-SLNs) the uptake was markedly higher than that of Cou 6-SLNs *(~ 2.5 folds higher)*, which was proposed to be the result of the targeting capacity of Lf through receptor-mediated endocytosis *via* Lf receptors expressed on MCF-7 cells. Quantitative analysis indicated results very similar to those obtained from fluorescence imaging.

3.7. In vivo assessment of different atorvastatin formulations' efficacy

3.7.1. Tumor volume

Numerous studies have examined the ability of various formulations to inhibit tumor growth by examining their impact on the cell cycle, often through methods such as measuring EdU uptake (Beckwitt et al., 2018; Marti et al., 2021). However, in the present study, a simpler and more cost-effective method was employed to assess the tumor growth inhibitory effect of different ATR formulations. Tumor volume measurements were taken every other day, starting from day 9 until the end of the study, as evidence of the inhibitory effects on tumor growth. Fig. 7 depicts the impact of different drug formulations on the growth of breast tumors. By the ninth day, all animals who had not received any treatment exhibited a clearly visible solid tumor in the mammary fat pad where Ehrlich cells were injected. Consequently, the tested drugs were administered starting from day 10. The tumor volume in the untreated mice exhibited continuous and gradual growth during the whole treatment period. The ATR Ca, ATR Ca-SLNs, and Lf-ATR Ca-SLNs treatments effectively reverted the development of tumor volume compared to the untreated group, over the whole follow-up period. On the 25th day, ATR Ca-SLNs, and Lf-ATR Ca-SLNs showed a significant superior effect in tumor volume reduction as compared to that caused by ATR *Ca.* However, the Lf-ATR Ca-SLNs caused the most significant decline in the tumor volume as compared to other treated groups. These results illustrate that loading SLNs with atorvastatin coated with lactoferrin is a promising treatment for breast cancer.

3.7.2. Histopathological assessments done for H &E-stained tumor sections

Fig. 8 illustrates the histopathological changes observed in hematoxylin and eosin (H and E) stained sections of breast mammary tissues upon induction of breast solid tumor induced by Ehrlich as well as the effect of all treatments given. The mammary fat pad of normal mice revealed normal breast lobules and ducts, (Fig. 8A). Furthermore, the untreated Ehrlich induced breast solid tumor group showed aggressive infiltrative tumors, atypical cells with basophilic cytoplasm and nuclei with pleomorphic hyperchromatic coarse chromatin, and mean number of mitotic bodies/10HPF = 62, (Fig. 8B). The experimental group that administered SLNs only showed histopathological features similar to that observed in the untreated Ehrlich induced breast solid tumor group, with mean number of mitotic cells/10HPF = 59 (Fig. 8C). The Lf-SLNs treated group showed a mild anti-tumor effect, with necrotic area of reaching about 10% and 50 mitotic bodies/10 HPF, (Fig. 8D). The ATR Ca treatment showed a moderate antitumor effect with better results observed in the higher dose used reaching necrotic areas of about 25, 40%, and mean number of mitotic cells/10 HPF = 40, 32, (Fig.8 E, F). Moreover, the ATR Ca-SLNs showed better anti-tumor effect than that observed in the ATR Ca treated mice reaching necrotic areas of about 64, 71%, and and mean number of mitotic cells/10 HPF = 21, 14 respectively (Fig. 8G & H). The Lf-ATR Ca-L-SLNs treated mice showed the best antitumor effect especially in the higher dose reaching necrotic areas of about 85, 95%, respectively and mean number of mitotic cells/10 HPF = 8, 0 (Fig.8 I, J). Fig. K represents a bar chart to illustrate the % of necrosis in assessed sections for various experimental groups.

3.7.3. Immunohistochemical Analysis of Caspase 3

Immunohistochemical assessment of apoptosis by the detection of caspase 3 revealed a significant difference among the tested groups. There was no significant difference between apoptotic activities within the negative control, positive control, and the blank solid lipid nanoparticles group (group 3). On the other hand, blank solid lipid nanoparticles decorated with Lf showed significantly enhanced apoptotic activity compared with negative control, positive control, and blank solid lipid nanoparticles. Moreover, a significant increase in the apoptotic activity was observed within the following groups compared to the control group: group 6: ATR Ca 10 mg/kg/day, group 8: whom were SLNs loaded with ATR Ca and given in dose (10 mg/kg/day) (ATR

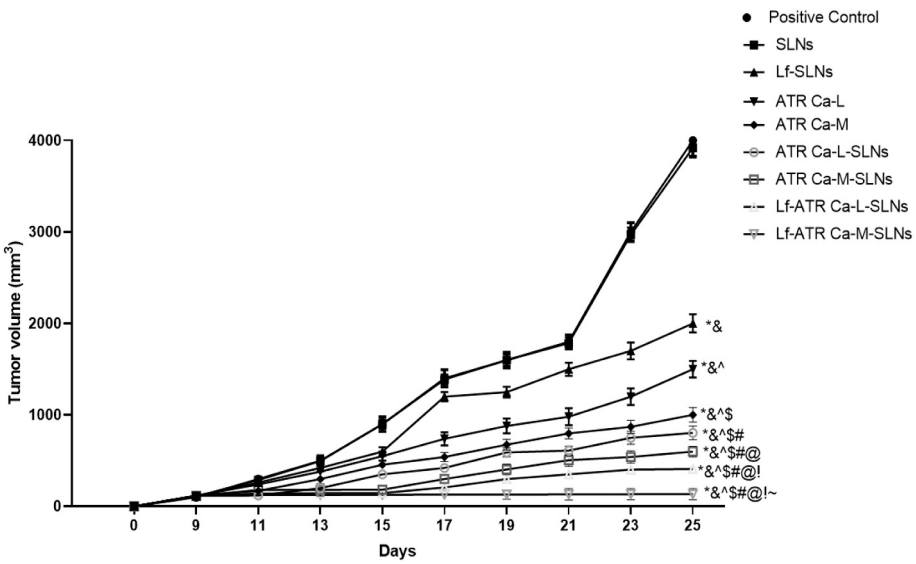

Fig. 7. The variations in the volume of tumor of Ehrlich induced solid breast cancer in mice after the treatment with SLNs, Lf-SLNs, ATR Ca at doses of (5, 10 mg/kg/day), ATR Ca-SLNs at doses of (5, 10 mg/kg/day), and Lf-ATR Ca-SLNs at doses of (5, 10 mg/kg/day) for 15 days. Each point represents the mean ± SD of 10 mice. *, is significantly different from positive control group, $P < 0.05$, †, is significantly different from the SLNs-treated group, $P < 0.05$. ††, is significantly different from the Lf-SLNs-treated group, $P < 0.05$. ¶, is significantly different from the ATR Ca-L-treated group, $P < 0.05$. §, is significantly different from the ATR Ca-M-treated group, $P < 0.05$. ||, is significantly different from the ATR Ca-L-SLNs-treated group, $P < 0.05$. #, is significantly different from the ATR Ca-M-SLNs-treated group, $P < 0.05$. ~, is significantly different from the Lf-ATR Ca-L-SLNs-treated group, $P < 0.05$.

Ca-M-SLNs), group 9: who were treated with ATR Ca-SLNs and decorated with Lf and given in dose 5 mg/kg/day (Lf-ATR Ca-L-SLNs), group 10: who were treated with ATR Ca-SLNs decorated with Lf and given in dose (10 mg/kg/day) (Lf-ATR Ca-M-SLNs), (Fig. 9).

Within the different proposed treatment formulations, the SLNs loaded with ATR Ca 10 mg/kg/day formulations either decorated/ undecorated with Lf (ATR Ca-M-SLNs & Lf-ATR Ca-M-SLNs) showed the best efficacy, with superior activity observed within the formulation decorated with Lf as shown in (Fig. 9). The antitumor activities of statins have been widely studied before. It was demonstrated that statins exert anti-tumor effects by targeting different cancer hallmarks in various types of cancer such as breast, bladder, and Lung cancer. Retrospective studies correlated statins use with decreased tumor-related mortality and poor prognosis (Sławińska and Kandefer-Szerszeń, 2008).

Several researchers investigated the mechanism of atorvastatin antitumor activity, it was observed that atorvastatin has the ability to inhibit the proliferation, invasion and epithelial-mesenchymal transition of breast cancer cells *via* the inhibition of PTEN/AKT pathway and over-expressing Ras homolog family member B (RhoB) which in turn lead to apoptosis induction in breast cancer cells (Ma et al., 2019). Recently, ATR Ca was shown to modulate the breast cancer tumor microenvironment and support the immune surveillance mechanism. Where Eun-Ji et al. (Choe et al., 2022) showed that atorvastatin can suppress PD-L1 tumor extracellular vesicles *via* the inhibition of extracellular vesicles' secretion and PD-L1 expression. In addition, it increased the immune antitumor response *via* activation the CD8+ T cells cytotoxicity, increased the activity of CD4+ T helper cells, and downregulation of regulatory T cells (Choe et al., 2022). Moreover, using lactoferrin as a targeting moiety in the designed atorvastatin formulations has provided atorvastatin with an add-on effect, where lactoferrin was shown previously to have antitumor properties. Several investigations reported that lactoferrin has the ability to selectively target cancer cells, inhibiting tumor proliferation, survival, invasion, and metastasis (Cutone et al., 2020). Furthermore, lactoferrin was shown to promote cancer cells' apoptosis *via* different mechanisms; including the direct activation of caspase 9 and caspase3, upregulation of different proapoptotic proteins such as Bid and Bax, and the activation of FAS apoptotic signaling pathway (Gibbons et al., 2015).

Lactoferrin's immunomodulatory effect within the tumor microenvironment makes it a promising antitumor strategy, where it was shown that lactoferrin has the ability to inhibit the proliferation of regulatory T cells and tumor-associated macrophage. It is capable also of enhancing the proliferation and activation of cytotoxic T cells, helper T cells, and natural killer cells. In addition, it was shown to modulate the microbiome population within the tumor microenvironment thus inhibiting tumor growth, invasion, and metastasis (Dong et al., 2020; El-Fakharany et al., 2022; Kondapi, 2020).

4. Conclusion

The present study demonstrates the successful preparation of surfactant-free lipid nanocarriers for the delivery of ATR—*Ca.* Loading ATR Ca-SLNs achieved high entrapment efficiency exceeding 90%, resulting in formulations with optimal colloidal properties and release profiles. When ATR Ca-SLNs were decorated with lactoferrin as a targeted drug delivery system for breast cancer, enhanced anti-tumor efficacy and accelerated cellular uptake by MCF-7 cells were observed compared to undecorated SLNs and free drug. *In vivo* assessment revealed promising anti-tumor activity for different atorvastatin formulations, both decorated and undecorated with lactoferrin. Among them, medium-dose formulations (ATR Ca-M-SLNs & Lf-ATR Ca-M-SLNs) demonstrated superior activity, with the Lf-decorated formulation exhibiting higher efficacy. These findings highlight the potential of our unique Lf-ATR Ca-SLNs as effective carriers for repurposed pharmaceuticals, including ATR *Ca.* Also, the recently developed nano-system addresses additional obstacles related to meeting international carrier toxicity and biocompatibility criteria. However, several challenges such as scalability, cost, and characterization need to be addressed to translate these technologies into clinically viable medicines. While the current study yielded promising results, it is important to acknowledge its limitations. The primary focus was on evaluating the clinical outcomes of the developed formulation specifically for the primary tumor, without investigation into the impact on dormant micrometastases or the development of other metastases. Additionally, the assessment of muscle injury in treated mice, which could have provided valuable insights, was not conducted due to limitations in facilities and expertise at the time of

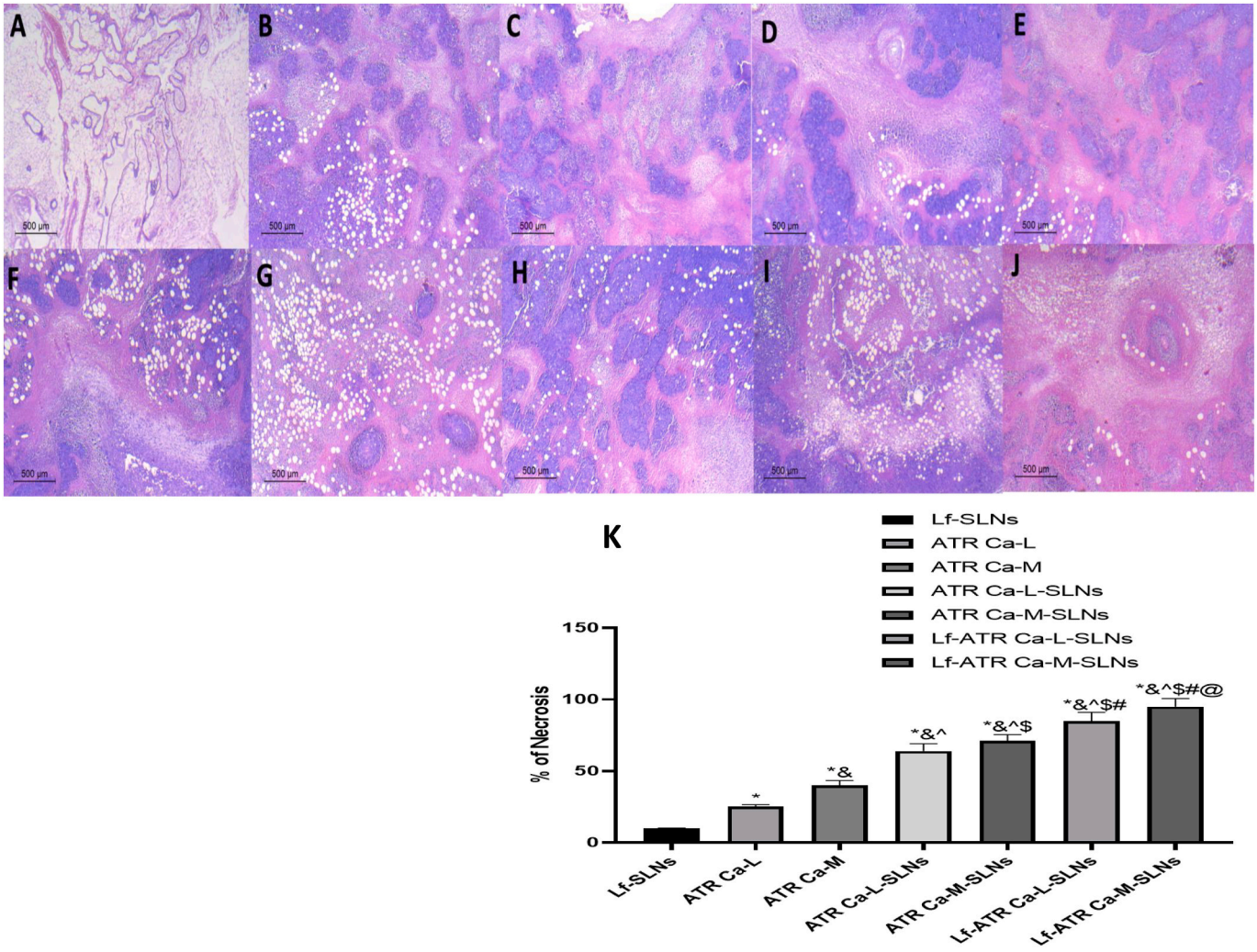

Fig. 8. The histopathological changes observed in ehrlich induced solid breast cancer in mice after treatment with SLNs, Lf-SLNs, ATR Ca at doses of (5, 10 mg/kg/day), ATR Ca-SLNs at doses of (5, 10 mg/kg/day), and Lf-ATR Ca-SLNs at doses of (5, 10 mg/kg/day) for 15 days.
A. The mammary fat pad of normal mice revealed normal breast lobules and ducts.
B. Positive control showing sheets of malignant cells.
C. The SLNs treated group showing similar results shown in the ehrlich untreated group.
D. The Lf-SLNs treated group.
E. ATR Ca treated group at low dose.
F. ATR Ca treated group at medium dose.
G. ATR Ca-SLNs treated group at low dose.
H. ATR Ca-SLNs treated group at medium dose.
I & J. Lf-ATR Ca-L-SLNs treated group at low and medium dose, respectively, showing variable degrees of anti-tumor and necrotic effects.
K. Bar chart representing area of necrosis in different experimental groups.
*, is significantly different from Lf-SLNs-treated group, $P < 0.05$, †, is significantly different the ATR Ca-L-treated group, $P < 0.05$. ††, is significantly different from the ATR Ca-M-treated group, $P < 0.05$. ¶, is significantly different from the ATR Ca-L-SLNs-treated group, $P < 0.05$. §, is significantly different from the ATR Ca-M-SLNs-treated group, $P < 0.05$. ||, is significantly different from the Lf-ATR Ca-L-SLNs-treated group, $P < 0.05$.

the study. Recognizing the importance of these investigations, they will be duly considered in future research.

Ethical approval

All animal study experimental procedures were performed in strict compliance with the standards for the care and use of laboratory animals (NIH), the animal research: reporting of in vivo experiments (ARRIVE) guidelines and approved by ethics committee at Pharos University in Alexandria (PUA) (PUA-01202311263150). Please find the attached ethical approval report as supplementary material.

Funding

The authors affirm that they did not receive any financial assistance, grants, or other forms of support or funds while preparing this manuscript.

CRediT authorship contribution statement

Dina M. Gaber: Writing – review & editing, Writing – original draft, Supervision, Methodology, Data curation, Conceptualization. **Sherihan S. Ibrahim:** Writing – original draft, Methodology. **Ashraf K. Awaad:** Writing – original draft, Methodology. **Yasmine M. Shahine:** Writing – review & editing, Writing – original draft. **Salma Elmallah:** Validation,

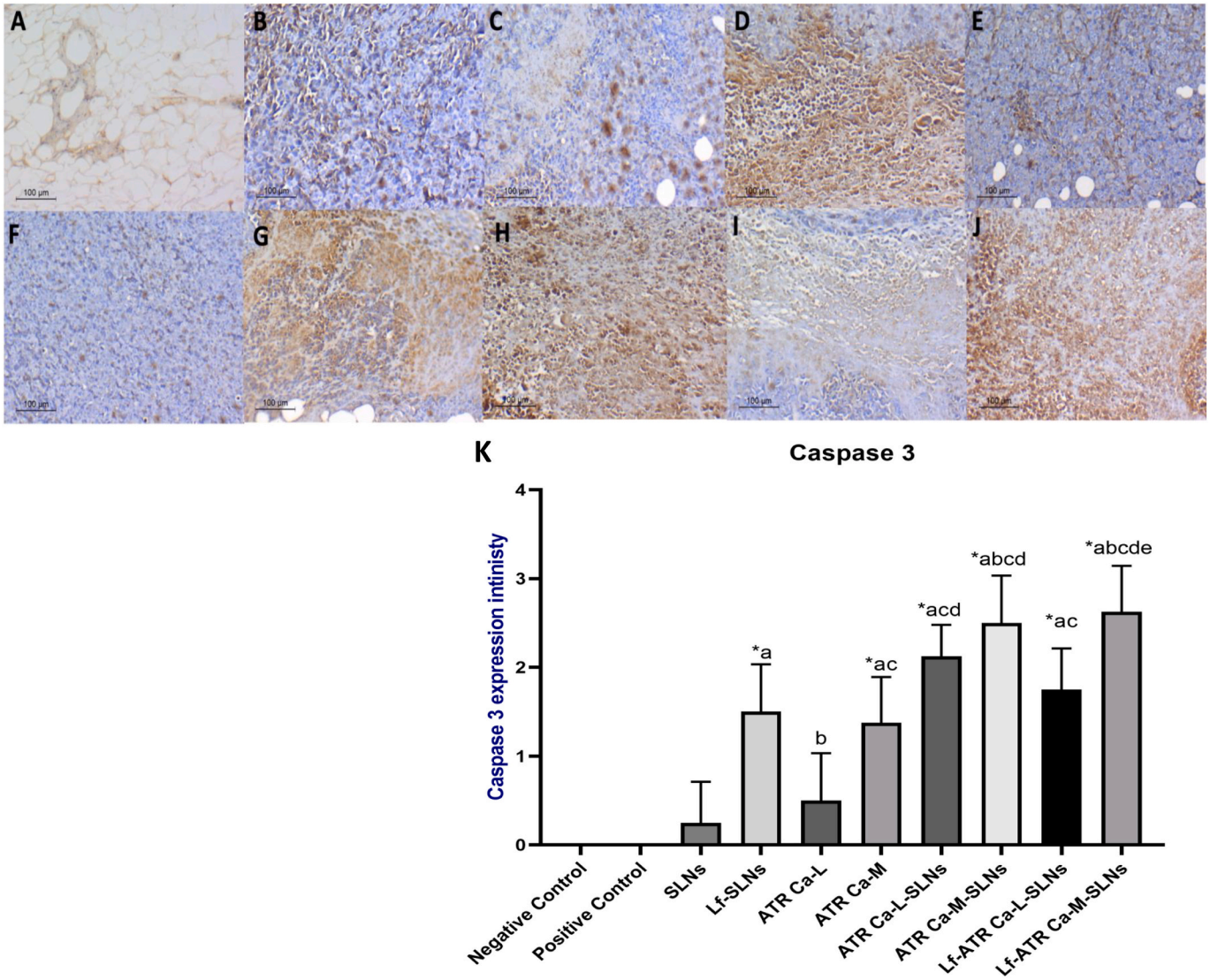

Fig. 9. Immunohistochemical analysis of caspase 3 within different animal groups (IHCx100).
A. Negative Caspase 3 staining within negative control group(−ve).
B. Negative caspase 3 staining within the positive control group (+ve).
C. Caspase 3 staining within SLNs blank formulation showing negative stating.
D. Caspase 3 expression in the Lf-SLNs group showing moderate expression mostly in stroma.
E. Negative caspase 3 staining in ATR Ca-L group.
F. Mild stromal caspase 3 staining within ATR Ca-M group with absence of nuclear staining.
G. Caspase 3 expression within ATR Ca-L-SLNs group showing moderate stromal staining accompanied by mild nuclear staining.
H. Caspase 3 expression within ATR Ca-M-SLNs group showing strong nuclear and cytoplasmic staining.
I. Moderate caspase 3 staining within Lf-ATR Ca-L-SLNs group.
J. Strong caspase 3 staining within Lf-ATR Ca-M-SLNs group.
K. Bar chart representing caspase 3 expression.
*, Significant *from -ve and + ve control,* †, *significant from SLNs,* ††, *significant from Lf-SLNs,* ¶, *significant from ATR Ca-L,* §, *significant from ATR Ca-M,* ||, *significant from ATR Ca-M-SLNs.*

Methodology, Formal analysis. **Hebatallah S. Barakat:** Writing – review & editing, Methodology. **Noha I. Khamis:** Writing – review & editing, Methodology.

Declaration of competing interest

The authors declare that they have no relevant financial or non-financial conflict of interest to disclose.

Data availability

The datasets produced and/or analyzed during the present study can be obtained from the corresponding author upon reasonable request.

Appendix A. Supplementary data

Supplementary data to this article can be found online at https://doi.org/10.1016/j.ijpx.2024.100249.

References

Abolghasemi, R., Ebrahimi-Barough, S., Bahrami, N., Aid, J., 2022. Atorvastatin inhibits viability and migration of MCF7 breast cancer cells. Asian Pacif. J. Cancer Prevent.: APJCP 23 (3), 867.

Abou Shousha, S., Baheeg, S., Ghoneim, H., Zoheir, M., Hemida, M., Shahine, Y., 2023. The effect of Fas/FasL pathway blocking on apoptosis and stemness within breast cancer tumor microenvironment (preclinical study). Breast Dis. 42 (1), 163–176.

Beckwitt, C.H., Clark, A.M., Ma, B., Whaley, D., Oltvai, Z.N., Wells, A., 2018. Statins attenuate outgrowth of breast cancer metastases. Br. J. Cancer 119 (9), 1094–1105.

Bhagwat, G.S., Athawale, R.B., Gude, R.P., Md, S., Alhakamy, N.A., Fahmy, U.A., Kesharwani, P., 2020. Formulation and Development of Transferrin Targeted Solid Lipid Nanoparticles for Breast Cancer Therapy. Front. Pharmacol. 11, 614290 https://doi.org/10.3389/fphar.2020.614290.

Cheng, Z., Li, M., Dey, R., Chen, Y., 2021. Nanomaterials for cancer therapy: current progress and perspectives. J. Hematol. Oncol. 14 (1), 1–27.

Choe, E.-J., Lee, C.-H., Bae, J.-H., Park, J.-M., Park, S.-S., Baek, M.-C., 2022. Atorvastatin enhances the efficacy of immune checkpoint therapy and suppresses the cellular and extracellular vesicle PD-L1. Pharmaceutics 14 (8), 1660.

Cutone, A., Rosa, L., Ianiro, G., Lepanto, M.S., Bonaccorsi di Patti, M.C., Valenti, P., Musci, G., 2020. Lactoferrin's anti-cancer properties: Safety, selectivity, and wide range of action. Biomolecules 10 (3), 456.

da Rocha, M.C.O., da Silva, P.B., Radicchi, M.A., Andrade, B.Y.G., de Oliveira, J.V., Venus, T., Merker, C., Estrela-Lopis, I., Longo, J.P.F., Báo, S.N., 2020. Docetaxel-loaded solid lipid nanoparticles prevent tumor growth and lung metastasis of 4T1 murine mammary carcinoma cells. J. Nanobiotechnol. 18, 1–20.

Dean, M., Fojo, T., Bates, S., 2005. Tumour stem cells and drug resistance. Nat. Rev. Cancer 5 (4), 275–284.

Devi, L., Gupta, R., Jain, S.K., Singh, S., Kesharwani, P., 2020. Synthesis, characterization and in vitro assessment of colloidal gold nanoparticles of Gemcitabine with natural polysaccharides for treatment of breast cancer. Drug Deliv. Sci. Technol. 56, 101565.

Dong, H., Yang, Y., Gao, C., Sun, H., Wang, H., Hong, C., Wang, J., Gong, F., Gao, X., 2020. Lactoferrin-containing immunocomplex mediates antitumor effects by resetting tumor-associated macrophages to M1 phenotype. J. Immunotherap. Cancer 8 (1), 1–12.

El-Fakharany, E.M., Ashry, M., Abd-Elaleem, A.-E.H., Romeih, M.H., Morsy, F.A., Shaban, R.A., Abdel-Wahhab, K.G., 2022. Therapeutic efficacy of Nano-formulation of lactoperoxidase and lactoferrin via promoting immunomodulatory and apoptotic effects. Int. J. Biol. Macromol. 220, 43–55.

El-Hawary, A.K., Abbas, A.S., Elsayed, A.A., Zalata, K.R., 2012. Molecular subtypes of breast carcinoma in Egyptian women: clinicopathological features. Pathol.-Res. Pract. 208 (7), 382–386.

El-Khashab, I.H., 2021. Antiangiogenic and proapoptotic activities of atorvastatin and ganoderma lucidum in tumor mouse model via VEGF and caspase-3 pathways. Asian Pacif. J. Cancer Prevent.: APJCP 22 (4), 1095.

Elzoghby, A.O., Abdelmoneem, M.A., Hassanin, I.A., Abd Elwakil, M.M., Elnaggar, M.A., Mokhtar, S., Fang, J.-Y., Elkhodairy, K.A., 2020. Lactoferrin, a multi-functional glycoprotein: active therapeutic, drug nanocarrier & targeting ligand. Biomaterials 263, 120355.

Etman, S.M., Abdallah, O.Y., Mehanna, R.A., Elnaggar, Y.S.R., 2020. Lactoferrin/Hyaluronic acid double-coated lignosulfonate nanoparticles of quinacrine as a controlled release biodegradable nanomedicine targeting pancreatic cancer. Int. J. Pharm. 578, 119097.

Gaber, D.M., Nafee, N., Abdallah, O.Y., 2017. Myricetin solid lipid nanoparticles: Stability assurance from system preparation to site of action. Eur. J. Pharm. Sci. 109 (May), 569–580. https://doi.org/10.1016/j.ejps.2017.08.007.

Gambhire, V.M., Salunkhe, S.M., Gambhire, M.S., 2018. Atorvastatin-loaded lipid nanoparticles: antitumor activity studies on MCF-7 breast cancer cells. Drug Dev. Ind. Pharm. 44 (10), 1685–1692. https://doi.org/10.1080/03639045.2018.1492605.

Gibbons, J.A., Kanwar, J.R., Kanwar, R.K., 2015. Iron-free and iron-saturated bovine lactoferrin inhibit survivin expression and differentially modulate apoptosis in breast cancer. BMC Cancer 15 (1), 1–16.

Ibrahim, S.S.A., El-Aal, S.A.A., Reda, A.M., El Achy, S., Shahine, Y., 2022. Anti-neoplastic action of Cimetidine/Vitamin C on histamine and the PI3K/AKT/mTOR pathway in Ehrlich breast cancer. Sci. Rep. 12 (1), 11514.

Jiang, W., Hu, J.-W., He, X.-R., Jin, W.-L., He, X.-Y., 2021. Statins: a repurposed drug to fight cancer. J. Exp. Clin. Cancer Res. 40, 1–33.

Kafle, U., Agrawal, S., Dash, A.K., 2022. Injectable Nano Drug delivery Systems for the Treatment of Breast Cancer. Pharmaceutics 14 (12), 2783.

Knoblaugh, S.E., Himmel, L.E., 2019. Keeping score: semiquantitative and quantitative scoring approaches to genetically engineered and xenograft mouse models of cancer. Vet. Pathol. 56 (1), 24–32.

Kondapi, A.K., 2020. Targeting cancer with lactoferrin nanoparticles: recent advances. Nanomedicine 15 (21), 2071–2083.

Kulkarni, S.A., Feng, S.-S., 2013. Effects of particle size and surface modification on cellular uptake and biodistribution of polymeric nanoparticles for drug delivery. Pharm. Res. 30, 2512–2522.

Kurmi, B.D., Gajbhiye, V., Kayat, J., Jain, N.K., 2011. Lactoferrin-conjugated dendritic nanoconstructs for lung targeting of methotrexate. J. Pharm. Sci. 100 (6), 2311–2320.

Liu, L., Ning, Y., Chen, C., Wang, D., 2009. Effect of atorvastatin on tumor growth and metastasis in a breast cancer cell xenograft model and its mechanism. Front. Med. China 3, 443–446.

Lochhead, P., Chan, A.T., 2013. Statins and colorectal cancer. Clin. Gastroenterol. Hepatol. 11 (2), 109–118.

Ma, Q., Gao, Y., Xu, P., Li, K., Xu, X., Gao, J., Qi, Y., Xu, J., Yang, Y., Song, W., 2019. Atorvastatin inhibits breast cancer cells by downregulating PTEN/AKT pathway via promoting ras homolog family member B (RhoB). Biomed. Res. Int. 2019, 1–15.

Malik, J.A., Ahmed, S., Jan, B., Bender, O., Al Hagbani, T., Alqarni, A., Anwar, S., 2022. Drugs repurposed: an advanced step towards the treatment of breast cancer and associated challenges. Biomed. Pharmacother. 145, 112375 https://doi.org/10.1016/j.biopha.2021.112375.

Marti, J.L.G., Beckwitt, C.H., Clark, A.M., Wells, A., 2021. Atorvastatin facilitates chemotherapy effects in metastatic triple-negative breast cancer. Br. J. Cancer 125 (9), 1285–1298.

Mekhail, G.M., Kamel, A.O., Awad, G.A.S., Mortada, N.D., 2012. Anticancer effect of atorvastatin nanostructured polymeric micelles based on stearyl-grafted chitosan. Int. J. Biol. Macromol. 51 (4), 351–363.

Misganaw, M., Zeleke, H., Mulugeta, H., Assefa, B., 2023. Mortality rate and predictors among patients with breast cancer at a referral hospital in Northwest Ethiopia: a retrospective follow-up study. PLoS One 18 (1), e0279656.

Moon, H., Ospina-Muñoz, N., Noe-Kim, V., Yang, Y., Elzey, B.D., Konieczny, S.F., Han, B., 2020. Subtype-specific characterization of breast cancer invasion using a microfluidic tumor platform. PLoS One 15 (6), e0234012.

Nafee, N., Gaber, D.M., Elzoghby, A.O., Helmy, M.W., Abdallah, O.Y., 2020. Promoted Antitumor activity of Myricetin against Lung Carcinoma Via Nanoencapsulated Phospholipid complex in Respirable Microparticles. Pharm. Res. 37 (82), 1–24.

Naik, N., Madani, A., Esteva, A., Keskar, N.S., Press, M.F., Ruderman, D., Agus, D.B., Socher, R., 2020. Deep learning-enabled breast cancer hormonal receptor status determination from base-level H&E stains. Nat. Commun. 11 (1), 5727.

Nosengo, N., 2016. Can you teach old drugs new tricks? Nature 534 (7607), 314–316.

Nour, E.M., El-Habashy, S.E., Shehat, M.G., Essawy, M.M., El-Moslemany, R.M., Khalafallah, N.M., 2023. Atorvastatin liposomes in a 3D-printed polymer film: a repurposing approach for local treatment of oral candidiasis. Drug Deliv. Transl. Res. 13 (11), 2847–2868.

Osmak, M., 2012. Statins and cancer: current and future prospects. Cancer Lett. 324 (1), 1–12.

Pandey, V., Gajbhiye, K.R., Soni, V., 2015. Lactoferrin-appended solid lipid nanoparticles of paclitaxel for effective management of bronchogenic carcinoma. Drug Deliv. 22, 199–205. https://doi.org/10.3109/10717544.2013.877100.

Pushpakom, S., Iorio, F., Eyers, P.A., Escott, K.J., Hopper, S., Wells, A., Doig, A., Guilliams, T., Latimer, J., McNamee, C., 2019. Drug repurposing: progress, challenges and recommendations. Nat. Rev. Drug Discov. 18 (1), 41–58.

Rivolta, I., Panariti, A., Lettiero, B., Sesana, S., Gasco, P., Gasco, M.R., Masserini, M., Miserocchi, G., 2011. Cellular uptake of coumarin-6 as a model drug loaded in solid lipid nanoparticles. J. Physiol. Pharmacol. 62 (1), 45.

Shilpi, S., Vimal, V.D., Soni, V., 2015. Assessment of lactoferrin-conjugated solid lipid nanoparticles for efficient targeting to the lung. Prog. Biomater. 4 (1), 55–63.

Sławińska, A., Kandefer-Szerszeń, M., 2008. The anticancer properties of statins. Adv. Hygien. Experim. Med. 62, 393–404.

Sung, H., Ferlay, J., Siegel, R.L., Laversanne, M., Soerjomataram, I., Jemal, A., Bray, F., 2021. Global cancer statistics 2020: GLOBOCAN estimates of incidence and mortality worldwide for 36 cancers in 185 countries. CA Cancer J. Clin. 71 (3), 209–249.

Talaat, S.M., Elnaggar, Y.S.R., El-Ganainy, S.O., Gowayed, M.A., Abdel-Bary, A., Abdallah, O.Y., 2022. Novel bio-inspired lipid nanoparticles for improving the anti-tumoral efficacy of fisetin against breast cancer. Int. J. Pharm. 628, 122184.

van Leeuwen, J.E., Ba-Alawi, W., Branchard, E., Cruickshank, J., Schormann, W., Longo, J., Silvester, J., Gross, P.L., Andrews, D.W., Cescon, D.W., 2022. Computational pharmacogenomic screen identifies drugs that potentiate the anti-breast cancer activity of statins. Nat. Commun. 13 (1), 6323.

Wang, W., Chen, T., Xu, H., Ren, B., Cheng, X., Qi, R., Liu, H., Wang, Y., Yan, L., Chen, S., 2018. Curcumin-loaded solid lipid nanoparticles enhanced anticancer efficiency in breast cancer. Molecules 23 (7), 1578.

Warita, K., Warita, T., Beckwitt, C.H., Schurdak, M.E., Vazquez, A., Wells, A., Oltvai, Z. N., 2014. Statin-induced mevalonate pathway inhibition attenuates the growth of mesenchymal-like cancer cells that lack functional E-cadherin mediated cell cohesion. Sci. Rep. 4 (1), 7593.

Was, H., Borkowska, A., Bagues, A., Tu, L., Liu, J.Y.H., Lu, Z., Rudd, J.A., Nurgali, K., Abalo, R., 2022. Mechanisms of chemotherapy-induced neurotoxicity. Front. Pharmacol. 13, 750507.

Wong, H.L., Bendayan, R., Rauth, A.M., Li, Y., Wu, X.Y., 2007. Chemotherapy with anticancer drugs encapsulated in solid lipid nanoparticles. Adv. Drug Deliv. Rev. 59 (6), 491–504.

Xu, P., Yu, H., Zhang, Z., Meng, Q., Sun, H., Chen, X., Yin, Q., Li, Y., 2014. Hydrogen-bonded and reduction-responsive micelles loading atorvastatin for therapy of breast cancer metastasis. Biomaterials 35 (26), 7574–7587.

Yaghmur, A., Mu, H., 2021. Recent advances in drug delivery applications of cubosomes, hexosomes, and solid lipid nanoparticles. Acta Pharm. Sin. B 11 (4), 871–885.

Zhang, Z., Gao, F., Bu, H., Xiao, J., Li, Y., 2012. Solid lipid nanoparticles loading candesartan cilexetil enhance oral bioavailability: in vitro characteristics and absorption mechanism in rats. Nanomedicine 8 (5), 740–747.